

Diffusion of interstitial hydrogen into and through bcc Fe from first principles

D. E. Jiang and Emily A. Carter

Department of Chemistry and Biochemistry, Box 951569, University of California, Los Angeles, California 90095-1569, USA

(Received 17 December 2003; revised manuscript received 12 May 2004; published 6 August 2004)

We report periodic spin-polarized density functional theory (DFT) predictions of hydrogen adsorption, absorption, dissolution, and diffusion energetics on and in ferromagnetic (FM) body-centered cubic (bcc) iron. We find that H prefers to stay on the Fe surface instead of subsurfaces or in bulk. Hydrogen dissolution in bulk Fe is predicted to be endothermic, with hydrogen occupying tetrahedral (t) sites over a wide range of concentrations. This is consistent with the known low solubility of H in pure Fe. In the initial absorption step, we predict that H occupies the deep subsurface t-site for Fe(110) and the shallow subsurface t-site for Fe(100). Diffusion of H into Fe subsurfaces is predicted to have a much lower barrier for Fe(100) than Fe(110). For H diffusion in bulk Fe, we find that H diffuses through bcc Fe not via a straight line trajectory, but rather hops from one t-site to a neighboring t-site by a curved path. Moreover, we exclude a previously suggested path via the octahedral site, due to its higher barrier and the rank of the saddle point. Quantum effects on H diffusion through bulk Fe are discussed.

DOI: 10.1103/PhysRevB.70.064102

PACS number(s): 66.30.Jt, 71.15.Mb, 71.15.Nc

I. INTRODUCTION

Hydrogen can greatly change the mechanical properties of structural metals and alloys and therefore cause material failure.^{1,2} Various mechanisms have been proposed to explain the H-induced embrittlement (HIE) of steels.³ However, because of its complexity, HIE remains an unsolved problem.⁴ Information about the atomic events occurring during H embrittlement are critical to understanding and modeling environmentally induced fracture, and ultimately may help suggest engineering solutions.

Iron or steel can absorb hydrogen during production, processing, and/or service. Many of those processes will produce adsorbed atomic hydrogen on Fe surfaces, which precedes the entry of hydrogen into the bulk. Fe(110) and Fe(100) are the two most stable low-index surfaces of Fe (lowest surface energy). Recently,⁵ we systematically studied with density functional theory (DFT) the adsorption of H on Fe(110) as a function of coverage; DFT predicts H to prefer the quasithreefold site on Fe(110), in agreement with low-energy electron diffraction (LEED) experiments.⁶ High-resolution electron energy-loss spectroscopy (HREELS) measurements indicate that H prefers the fourfold site on Fe(100),⁷ in agreement with early Hartree-Fock cluster predictions by Walch.⁸ However, this cluster work predicted the twofold site to be ~ 1.25 eV higher in energy than the fourfold site, contradicting recent periodic DFT-GGA (generalized gradient approximation) calculations by Eder, Terakura, and Hafner.⁹ They predicted H to prefer the twofold site on Fe(100), with the fourfold site only slightly less stable. We will use a different DFT approach here to revisit H on Fe(100), given the discrepancy between experimentally inferred and earlier DFT site preferences.

Chemisorbed H atoms on Fe surfaces can diffuse into the subsurface layers and then further into bulk Fe. Experimental work on H penetration has been done on Fe films, but not on specific crystal faces. Here we compare penetration pathways of H into Fe(110) and Fe(100).

After H is absorbed into bulk Fe, the next issue is where H atoms reside in the metal lattice. Due to the low solubility

and high mobility of hydrogen in iron and the high probability of trapping at defect sites at low temperatures, little direct evidence for the site occupancy exists. Indirect evidence indicates that H resides in the tetrahedral (t) site of body-centered cubic (bcc) Fe.¹⁰ However, conflicting theoretical predictions of both site preferences and the direction of charge transfer have been reported. Geometrical factors,¹¹ lattice relaxations,¹² and electronic arguments¹³ have been invoked to explain the site preference of H in bulk transition metals, though no universal theory can explain all cases.

In 1982, Nørskov found the t-site to be preferable, using the semiempirical effective medium theory (EMT),¹⁴ without allowing lattice relaxation. In 1984, using EMT, but also including lattice relaxations and a quantum mechanical treatment of the atomic motion of the H impurity, Puska and Nieminen¹⁵ found the octahedral (o) site and t-site to be almost degenerate in energy. Semiempirical extended Hückel (EH) studies by Companion and Liu¹⁶ (in 1985, with H in a rigid Fe cluster), Minot and Demangeat¹⁷ (in 1987, with a rigid periodic crystal), and Juan and Hoffmann¹⁸ (in 1999, with a periodic crystal and allowing just a breathing mode for the first Fe neighbors of H for lattice relaxation) predicted that H prefers the t-site over the o-site. By contrast, in 1989, Gong, Zeng, and Zheng¹⁹ found that H prefers the o-site by 0.11 eV over the t-site, using the spin-polarized $X\alpha$ method within a rigid cluster-in-cluster model. As for charge transfer, Minot and Demangeat predicted the direction to be from H to Fe, while Juan and Hoffmann found ~ 0.4 e charge transfer from Fe to H. Gong, Zeng, and Zheng found ~ 0.12 e and ~ 0.16 e transferred from Fe to t-site H and o-site H, respectively. In 2002, Miwa and Fukumoto²⁰ employed DFT-GGA with ultrasoft pseudopotentials (USPP).²¹ Using a Fe_{16}H supercell with the cell shape and volume fixed at the value predicted for bulk bcc Fe (2.851 Å), they found the t-site ~ 0.18 eV more stable than the o-site after ionic relaxation. All work mentioned above only explored one or two concentrations of H in Fe and most of them used less than 20 Fe atoms in the model, corresponding to a concentration of H

that is far too high. The solubility of H in Fe is very small (0.01 at.% at 1000 K and less than 3×10^{-6} at.% at room temperature²²). Therefore, it is critical to examine the concentration (or cell-size) convergence of properties to find a suitable concentration that realistically simulates H in Fe; this was lacking in previous studies and is one focus in the present work.

What distinguishes H from other deleterious impurities in transition metals is its high mobility. At room temperature, the diffusivity of H in pure bcc iron is about $1.0 \times 10^{-4} \text{ cm}^2 \text{ s}^{-1}$, compared to $1.0 \times 10^{-16} \text{ cm}^2 \text{ s}^{-1}$ for carbon and nitrogen.²³ Whether or not HIE happens by accumulation of gaseous hydrogen, formation of hydrides, localized plastic deformation, or reduction of cohesion, all of these postulated mechanisms³ are enabled by the high diffusivity of hydrogen. In principle, quantum tunneling could also contribute to H's high diffusivity in bcc Fe. Extensive experimental investigations of H diffusion have been carried out on various irons and steels.²⁴ However, direct evidence of the diffusion path is still lacking due to inherent limitations in spatial and time resolution of experimental techniques, which do not permit probing of individual reactive events in solids (not to mention the difficulty associated with probing a transition state in condensed matter). Periodic DFT coupled with a solid-state transition-state search algorithm provides a way to study the atomic mechanism of solid-state diffusion. The success of such studies^{25–28} on other materials encourages us to work on hydrogen diffusion into and through iron.

In this work, we use periodic DFT to investigate site preferences for H on Fe(100), in Fe(110) and Fe(100) subsurfaces, and in bulk Fe. We then go on to investigate how H diffuses into Fe(110) and Fe(100) subsurfaces. Next, we identify the nature of the classical, thermally activated path H takes to diffuse in bcc Fe. The rest of the paper is organized as follows. Section II describes the theoretical method employed, Sec. III presents the results and discussion, and Sec. IV provides a summary and conclusions.

II. THEORETICAL METHOD

We performed DFT^{29,30} calculations within the generalized gradient approximation of the PBE form³¹ for electron exchange and correlation, using the Vienna Ab Initio Simulation Package.^{32–34} Here we employed Blöchl's projector-augmented wave (PAW) method,³⁵ as implemented by Kresse and Joubert.³⁶ The PAW method is an all-electron DFT technique (within the frozen-core approximation) with the computational efficiency of pseudopotential techniques. We tested k -point sampling and kinetic energy cutoff convergence for all supercells. As a result of the convergence tests, we use a kinetic energy cutoff of 350 eV for all calculations. Structural relaxations were performed until forces on each atom were below 0.01 eV/Å. Using a $15 \times 15 \times 15$ k -point mesh for the primitive cell, we obtain for bcc Fe a lattice constant of 2.834 Å, a bulk modulus of 174 GPa, a local magnetic moment of 2.20 μ_B , which agree very well with experiment³⁷ and previous DFT-GGA-FLAPW results.³⁸

For the study of H/Fe(110), we use a $p(2 \times 2)$ surface cell and a k -point sampling of $7 \times 7 \times 1$. For H/Fe(100), we use

a k -point sampling of $12 \times 12 \times 1$, $6 \times 6 \times 1$, and $4 \times 4 \times 1$ for the $p(1 \times 1)$ (for 1.0 ML coverage), $p(2 \times 2)$ (for 0.25 ML coverage), and $p(3 \times 3)$ (for 0.11 ML) surface cell, respectively. When modeling Fe(110), we use seven layers of Fe atoms, with the bottom four layers fixed at their bulk positions; when modeling Fe(100), we use five layers of Fe atoms, with the bottom three layers fixed at their bulk positions. We use a 10 Å thick vacuum layer for both Fe(110) and Fe(100). We allow the H layer, together with the top three layers of the Fe(110) slab or the top two layers of the Fe(100) slab, to relax. For the more open Fe(100) surface, allowing one more Fe layer (the middle layer) to relax only causes a 5 meV change in total energy; therefore, the original number of layers allowed to relax should be sufficient. For all the subsurface calculations, we use 0.25 ML of H for both Fe(110) and Fe(100).

For H in bulk Fe calculations, we use a k -point sampling of $12 \times 12 \times 12$, $6 \times 6 \times 6$, $4 \times 4 \times 4$, and $2 \times 2 \times 2$ for Fe₂, Fe₁₆, Fe₅₄, and Fe₁₂₈, respectively, which converges the dissolution energy to within 0.03 eV for each (unrelaxed) cell. The first-order Methfessel-Paxton method³⁹ is used for the Fermi-surface smearing in order to obtain accurate forces, and a smearing width of 0.1 eV is chosen such that the error in the extrapolated energy at 0 K is less than 1 meV/atom. Both the cell-shape and atomic positions in bulk cells are allowed to relax.

The dissolution energy of hydrogen atoms in bulk Fe, the adsorption energy of hydrogen atoms on Fe surfaces, and the absorption energy into Fe subsurface sites are defined in the same manner, as given in Eq. (1).

$$\Delta E = E(\text{Fe}_n\text{H}) - E(\text{Fe}_n) - \frac{1}{2}E[\text{H}_2(\text{g})]. \quad (1)$$

Here all energies are referenced to the gaseous hydrogen molecule and pure Fe. The first term on the right-hand side is the total energy of the supercell that includes n Fe atoms and 1 H atom; the second term is the total energy of the supercell that consists of n Fe atoms. The first two terms are calculated with the same parameters (k -point sampling, energy cutoff, etc.). The third term is half the total energy of the hydrogen molecule, which is calculated by putting H₂ in a cubic box with 10 Å sides and carrying out a Γ -point calculation. We obtain for H₂ a bond length of 0.750 Å, a vibrational frequency of 4300 cm⁻¹, and a binding energy (D_e) of 4.54 eV, which are almost identical to previous GGA results⁴⁰ and in fairly good agreement with experimental values⁴¹ of 0.741 Å, 4395 cm⁻¹, and 4.75 eV.

The Climbing Image Nudged Elastic Band (CI-NEB) method⁴² is used to locate the minimum energy paths (MEPs) and the transition states for diffusion of H into Fe from Fe(110) and Fe(100) [using the surface $p(2 \times 2)$ cell] and for diffusion of H in bulk Fe (using the Fe₁₂₈ supercell). The NEB method⁴³ is a reliable way to find the MEP, when the initial and final states of a process are known. An interpolated chain of configurations (images) between the initial and final positions is connected by springs and relaxed simultaneously to the minimum energy path (MEP). With the climbing image scheme, the highest-energy image climbs uphill to the saddle point. When we use the CI-NEB method in

TABLE I. PAW-GGA(PBE) DFT adsorption energies (E_{ad}) and H-surface distances (d) for hydrogen atoms on Fe(100). The nature of the critical point is given in parentheses (min=minimum, hos=higher order saddle point). Zero-point-energy corrections are not included here.

Method		on-top	bridge	hollow
Current work				
$\theta=1$ ML ^a	E_{ad} (eV)	+0.45 (hos)	-0.24 (min)	-0.40 (min)
	d (Å)	1.56	0.93	0.35
$\theta=0.25$ ML	E_{ad} (eV)	+0.23 (hos)	-0.32 (min)	-0.38 (min)
	d (Å)	1.58	1.10	0.37
$\theta=0.11$ ML	E_{ad} (eV)	+0.20 (hos)	-0.34 (min)	-0.38 (min)
	d (Å)	1.58	1.20	0.37
USPP-GGA ^b				
$\theta=0.25$ ML	E_{ad} (eV)	+0.17	0.36	-0.35
	d (Å)	1.63	1.08	0.35

^aA monolayer (ML) is defined as one adsorbate atom per surface atom.

^bRef. 9.

this study, all the images are relaxed until the maximum force acting on an atom is less than 0.01 eV/Å. The ranks of the saddle points are determined by diagonalizing a finite difference construction of the Hessian matrix with displacements of 0.01 Å (allowing only H to move). Fe atoms are kept fixed. The zero-point energy (ZPE) is obtained by summing up the zero-point vibrational energies of the H's normal modes, i.e., $ZPE = \frac{1}{2} \sum_j \hbar \nu_j$, where ν is a real normal mode frequency.

III. RESULTS AND DISCUSSION

A. Hydrogen adsorption on Fe(110) and Fe(100)

In our earlier work,⁵ we examined hydrogen adsorption on Fe(110), finding that H prefers the quasithreefold site on Fe(110) at all coverages (0.25–1.0 ML). The DFT-GGA(PBE) adsorption energy of H on Fe(110) [as defined by Eq. (1)] was predicted to be -0.71 eV/atom, over the range examined. Here we compare our findings for H atom adsorption on Fe(100) with earlier theoretical and experimental results, as well as to the H/Fe(110) results. Table I displays the adsorption energy and the H-surface distance at $\theta_H=0.11$, 0.25, and 1 ML (the unit for the coverage ML is defined in Table I), after the structure of the H/Fe(100) slab is relaxed. For all coverages examined, the fourfold hollow site is found to be the lowest in energy, in agreement with what available experimental results suggested⁷ and with early Hartree-Fock cluster predictions by Walch.⁸ The on-top site is predicted to be endothermic with respect to gaseous H₂ and a clean Fe surface. By calculating the frequency spectrum for the H adatom on a Fe(100) surface fixed at the relaxed H/Fe(100) geometry, we find that both the twofold bridge and the fourfold hollow sites are true minima, while the on-top site is a rank-2 saddle point with two imaginary frequencies. Reducing the H coverage from

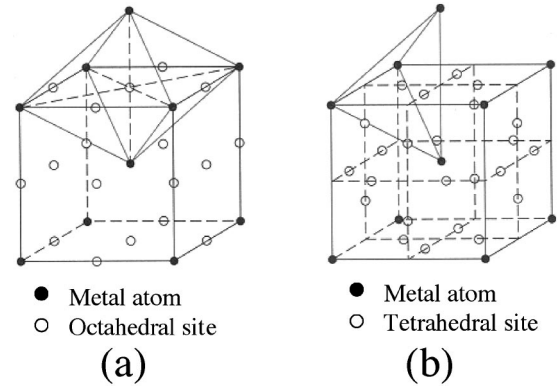


FIG. 1. The interstitial sites in a bcc lattice.

1 ML to 0.25 ML, the H adsorption energy changes only by 0.02 eV for the hollow site, but decreases significantly for the on-top and bridge sites. We can understand this trend by noting that hollow site H's have very small H-surface distances; any lateral repulsion is effectively screened by Fe atoms. By contrast, the other sites have much larger H-surface distances and lateral repulsions between H's are no longer screened by the substrate, leading to significant destabilization of the adsorbate at higher coverages. Further reducing the H coverage from 0.25 ML to 0.11 ML, the adsorption energy remains the same for the hollow site and changes by ~ 0.03 eV for the on-top and bridge sites. Since 0.03 eV is estimated to be the numerical error associated with our energetics, the adsorption properties of H/Fe(100) may be considered to be unchanging below 0.25 ML and therefore we use it for the following subsurface studies. Our results at 0.25 ML are similar to those reported by Eder, Terakura, and Hafner [USPP-GGA(PW91)],⁹ aside from their predicted near degeneracy between bridge and hollow site adsorption. The all-electron PAW method should be more accurate than the USPP method for transition metals, such as Fe, which may explain the better agreement between our results and the experimental indication that H occupies the hollow site. Compared with Fe(110), we found that H binds ~ 0.3 eV less strongly to Fe(100).

B. H in bcc Fe: Site preference and dissolution energy

Figure 1 displays the two types of interstices in the bcc lattice: tetrahedral (t) and octahedral (o). Using the experimental lattice parameter of bcc Fe (2.86 Å), the “radii” of the t-site and o-site are 0.36 Å and 0.19 Å, respectively. H has a covalent radius of 0.37 Å, so we would expect it will fit better in the t-site. Table II shows how the energy difference between o-site and t-site occupancy of H in bcc Fe converges with the supercell size, i.e., as the concentration of H becomes lower. We allow both cell shape and atomic positions to relax. The Fe₂H cell may be considered a supersaturated solution of H in Fe, or as an iron hydride. Both the unrelaxed and relaxed energy differences converge to within 10 meV at the Fe₁₆ supercell. For the four supercells (i.e., concentrations) we explored, Table II clearly shows that the t-site is always more stable, both for the unrelaxed and relaxed structures. Although the o-site occupancy gains more

TABLE II. The energy difference ($\Delta E = E_o - E_t$) between H in the o-site and t-site of bcc Fe for both unrelaxed and relaxed structures (for the unrelaxed structure, $a = 2.86 \text{ \AA}$).

Supercell	ΔE , unrelaxed (eV)	ΔE , relaxed (eV)
Fe ₂ H	0.51	0.01
Fe ₁₆ H	0.47	0.13
Fe ₅₄ H	0.46	0.13
Fe ₁₂₈ H	0.47	0.13

stabilization from lattice distortion than the t-site does, it still remains 0.13 eV higher in energy at all reasonable concentrations. When we examine the details of the relaxation for Fe₁₆H, we find that the cell remains the same shape and only the first coordination shell (four Fe atoms) around H moves outward by 0.06 Å when H is present in the t-site. This demonstrates that H fits well in the t-site. When H is put in the o-site, we find that both the cell shape and the first coordination shell around H undergo a tetragonal distortion. The cell c/a ratio changes to 1.033 from 1.000, while the two closest (axial) Fe atoms in the first coordination shell move outward by 0.17 Å and the four-less-close Fe atoms (equatorial) move inward by 0.03 Å. This distortion also propagates to the second and third coordination shells. Therefore, H in the o-site experiences a greater structural distortion than H in the t-site does, which agrees with the above analysis of site sizes. This required distortion is likely why the o-site is less stable than the t-site.

In order to see if any electronic factors contribute to relative site stability, we examined the charge density difference for both t-site and o-site occupancies of the unrelaxed Fe₁₆H cell (the minimum cell size where properties are converged) and found charge transfer from Fe to H. Regions of large charge depletion around Fe atoms are rather localized and limited to the first coordination shell of H. By integrating the charge density difference around H atom with a cutoff radius of 0.8 Å (which we find gives the largest amount charge transfer), $\sim 0.12 e$ and $\sim 0.11 e$ are predicted to transfer from Fe to H for the o-site and t-site, respectively. Thus a difference in the amount of charge transfer is not the reason for the site preference. The amount of charge transfer we find agrees

with Gong, Zeng, and Zheng's $X\alpha$ results,¹⁹ but is significantly lower than Juan and Hoffmann's EH results.¹⁸ Of the two previous studies, $X\alpha$ in general could be considered superior to EH (which is basically tight-binding). Philipp *et al.*¹³ found a correlation between the crystal electrostatic potential and the occupation of interstitial sites by H in bulk metals. They found that the t-site preference of H in bcc V, Nb, and Ta, and the o-site preference of H in fcc Pd could be correlated qualitatively with pure bulk metal's protonic electrostatic potential (i.e., the potential seen by a proton), which had its lowest value at the respective sites. However, since we find the H in bulk Fe to be neutral to slightly hydridic, we do not think such an analysis is relevant here.

Table III shows how the dissolution energy (essentially the heat of solution) of hydrogen in an Fe lattice converges with the supercell size, i.e., how it varies with concentration. The lowering in energy by relaxation is not large, only ~ 0.10 eV for cells larger than Fe₁₆, indicating again that H fits well in the t-site. The still-positive dissolution energy after relaxation demonstrates that the dissolution of hydrogen in bcc Fe is endothermic, consistent with the low solubility of H in bcc Fe. As the concentration of H decreases, the dissolution energies for both the relaxed and unrelaxed structures first decrease, reaching a minimum at Fe₁₆H, and then increase slightly. This increase after Fe₁₆H is about the same magnitude as the numerical error in our calculations, which is estimated to be ~ 0.02 eV, so we do not consider this "minimum" in ΔE to be numerically significant. The dissolution energies for relaxed structures vary only slightly with H concentration (essentially converged at ~ 0.20 eV for Fe₅₄H), which indicates that H-H repulsions are essentially non-existent. The volume expansion actually is very small (0.06%) for Fe₁₂₈ after a H atom is inserted in the lattice. In order to compare with experiment, we evaluated the ZPE correction to the dissolution energy. Assuming the Fe atoms to have infinite mass (i.e., the Fe atoms are fixed at their equilibrium positions), the ZPE of H in the Fe₁₂₈ cell is estimated to be 0.234 eV/atom. The ZPE of $1/2 H_2$ is 0.133 eV and therefore, the ZPE-corrected dissolution energy is calculated to be 0.301 eV/atom, which agrees extremely well with experimental value¹⁰ of 0.296 eV/atom and previous USPP-DFT-GGA results by Miwa and Fukumoto.²⁰

TABLE III. Dissolution energies (ΔE) of hydrogen in the t-site of bcc Fe with decreasing H concentration (C_H) for both unrelaxed and relaxed structures (for the unrelaxed structure, $a = 2.86 \text{ \AA}$) and percent change in volume (ΔV). For the theoretical dissolution energies, the ZPE-corrected values are in parentheses.

Method	Supercell	C_H (at. %)	ΔE , unrelaxed (eV)	ΔE , relaxed (eV)	ΔV (%) ^a
Current work	Fe ₂ H	33	0.45	0.20	11.5
	Fe ₁₆ H	5.9	0.27	0.16	2.10
	Fe ₅₄ H	1.8	0.28	0.19	0.57
	Fe ₁₂₈ H	0.78	0.29	0.20(0.30)	0.06
USPP-GGA ^b	Fe ₁₆ H	5.9		0.19(0.30)	
Experiment ^c				0.296	

^aThe volume increase of the relaxed Fe_nH cell with respect to the relaxed Fe_n cell.

^bRef. 20.

^cRef. 10.

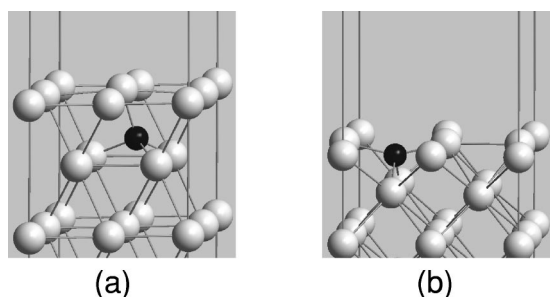


FIG. 2. (a) H in the t-site of the Fe(110) subsurface and (b) H in the t-site of the Fe(100) subsurface (H in dark and Fe light gray).

C. Hydrogen absorption in the subsurface of Fe(110) and Fe(100)

After finding the site preferences for H on Fe(100) and Fe(110) and in bulk Fe, we determined the relative stabilities of sites for H just below the surface and the barriers to accessing those sites from the surface. Since the number of the nearest-neighbor Fe atoms is the same for H in subsurface sites as for H in bulk Fe, it is not particularly surprising that H prefers the t-site to the o-site in the subsurface region, just as in the bulk. However, as we will see, the relative equilibrium positions of H atoms in the subsurface regions differ substantially from that in bulk Fe, as does the magnitude of the energy difference between the o-site and the t-site.

Two types of t-sites exist between the surface- and subsurface-layer Fe atoms of Fe(110). The first type consists of three Fe atoms from the surface layer and one from the subsurface layer, while the second type includes one Fe atom from the surface layer and three from the subsurface layer. The first type is closer to the surface than the second type. We found that the H atom spontaneously moves up to the surface threefold site after it is initially placed in the first type of t-site, indicating that there is no local minimum for that type of t-site. However, the second type of t-site is a local minimum for H. There is only one type of o-site in the subsurface region of Fe(110). Its energy is only ~ 0.02 eV higher than the t-site. This energy difference is smaller than in bulk Fe (~ 0.13 eV). The reason may be that the distortion caused by the o-site occupancy of H in the Fe(110) subsurface is reduced because three Fe atoms of the first coordination shell of H are in the surface layer. For Fe(100), there is only one type of t-site, and it is a local minimum for H. The o-site closest to the Fe(100) surface exists within the subsurface Fe layer; its energy is ~ 0.50 eV higher than the t-site.

Figure 2 displays the structures of the two subsurface t-sites for Fe(110) and Fe(100), which are local minima, and Table IV contains the structural parameters for the two sites. We predict that H is buried deeply in the subsurface of Fe(110), with the surface Fe atom coordinated to H being pushed toward vacuum by 0.16 Å. The subsurface site of H in Fe(100) is only slightly below the surface layer, with the two surface Fe atoms coordinated to H pushed apart laterally by 0.21 Å.

Now that we have established site preferences for H on Fe(110) and Fe(100) and in their respective subsurface regions, we now characterize the diffusion path that H may

TABLE IV. The H-surface distance (d_{H-S}) and the closest H-Fe distance (d_{H-Fe}) for hydrogen in subsurface t-sites of Fe(110) and Fe(100).

	Fe(110)	Fe(100)
d_{H-S} (Å)	1.46	0.35
d_{H-Fe} (Å)	1.66	1.68

follow to go from surface to subsurface. First, we sketch the energy landscape for H in the bulk, surface, and subsurface in Fig. 3, with the energy of a thick slab of Fe plus one half of an isolated H_2 molecule set as zero. We can see that H adsorption on Fe(110) is 0.71 eV exothermic, while H absorption in the subsurface of Fe(110) is 0.29 eV endothermic. H adsorption on Fe(100) is 0.38 eV exothermic, and H absorption in the subsurface of Fe(100) is 0.04 eV exothermic. Figures 4(a) and 4(b) show how H can diffuse into Fe(110) and Fe(100) subsurfaces, respectively. H has to overcome a barrier of 1.02 eV on Fe(110) and 0.38 eV on Fe(100) to diffuse into the subsurface, due to the significant endothermicity (1.00 and 0.34 eV) encountered in each case. This demonstrates that it is much easier for H to diffuse into the subsurface of Fe(100) than that of Fe(110), probably due to the lower packing density of the Fe(100) surface. The reverse process, i.e., surfacing of H from the subsurface, has a barrier of 0.02 eV for Fe(110) and 0.04 eV for Fe(100), indicating the ease with which H can move from subsurface to surface regardless of surface orientation.

After H goes into the subsurface, H can penetrate deeper and reach a bulk environment. Figure 3 shows that it is downhill by ~ 0.10 eV for H to go from the Fe(110) subsurface into the bulk, while it is uphill by ~ 0.24 eV for Fe(100). As we shall see in the next section, the intrinsic

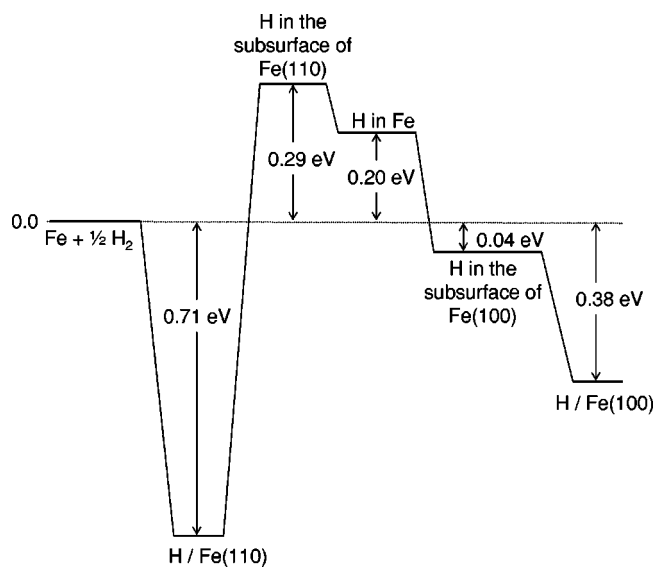


FIG. 3. Energy landscape for H in bulk Fe, and the surfaces and subsurfaces of Fe(110) and Fe(100). Zero-point energies are excluded. The energy of a thick slab of Fe (labeled here simply as Fe) with either (110) or (100) surfaces plus one-half of an isolated H_2 molecule is set as zero.

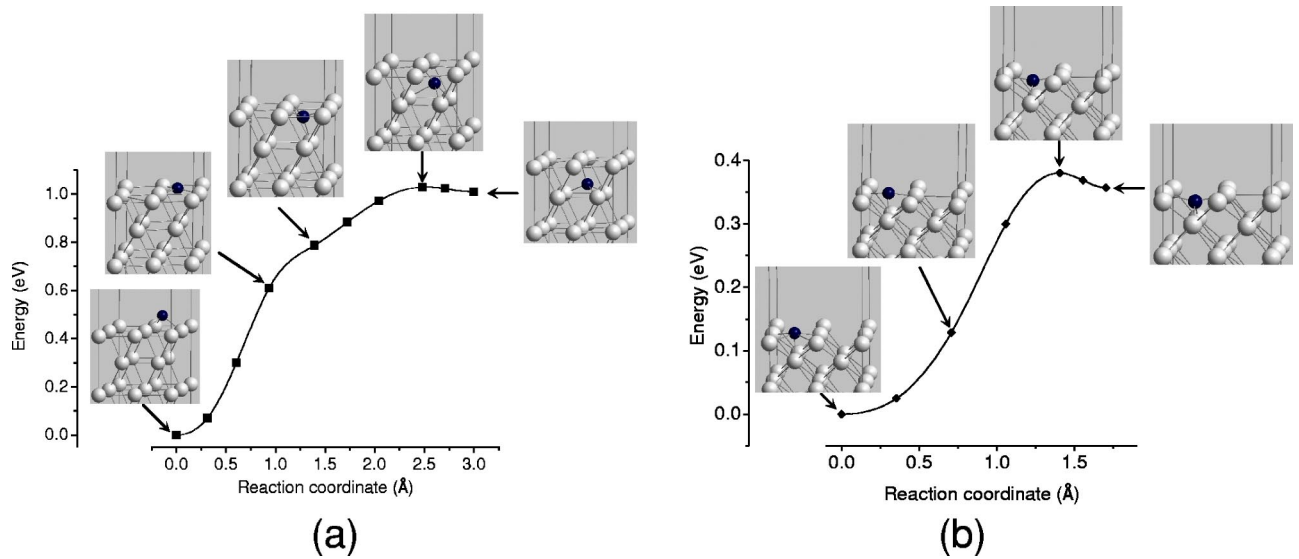


FIG. 4. Minimum energy path for hydrogen diffusion into the Fe subsurface region and several intermediate structures along the path: (a) into Fe(110) and (b) into Fe(100) (H in dark and Fe in light gray). Note the difference in scales between axes in (a) and (b).

barrier for bulk H diffusion is <0.05 eV; therefore it is sufficient to approximate the barriers by the endothermicity between reaction steps. Therefore, the large initial barrier for H to go into the subsurface of Fe(110) inhibits H incorporation, while the two relatively small barriers (~ 0.30 eV) allow H to be more easily incorporated via the (100) surface.

D. Hydrogen diffusion through FM bcc Fe

Given that H has already diffused into bulk Fe from the surface, we now investigate various possible diffusion paths in bulk Fe that H may follow, using a Fe_{128} supercell. We first considered a direct hopping path between two neighboring t-sites. Referring to Fig. 5(a), such a path involves H

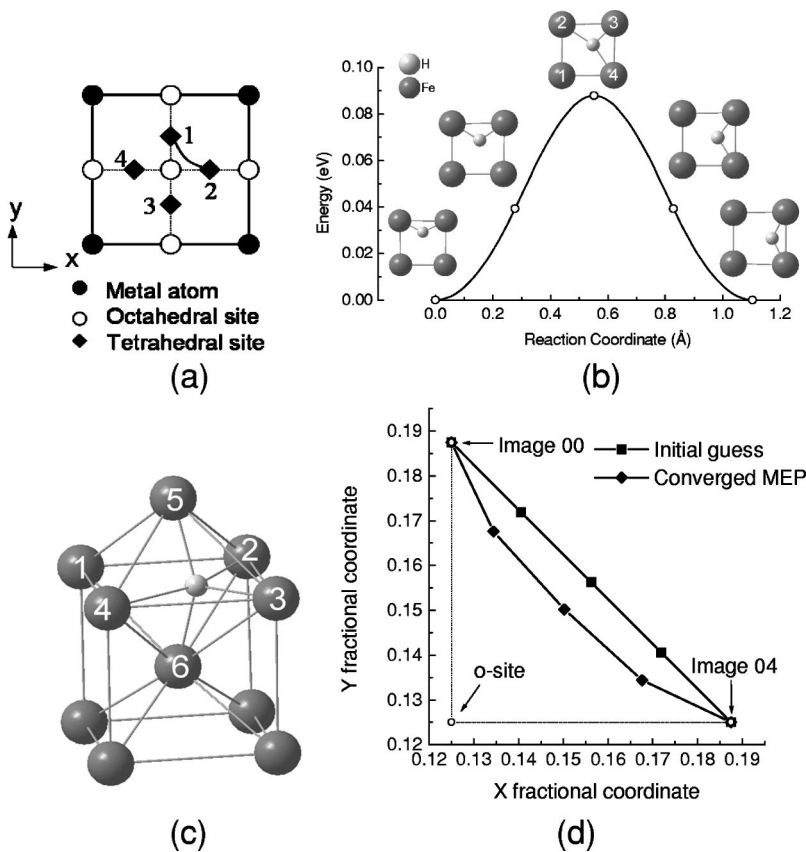


FIG. 5. (a) o-sites and t-site on the (001) plane of the bcc lattice, (b) energy profile and local structures for H diffusion from one t-site to a nearest-neighbor t-site, (c) structure of the transition state, and (d) initial guess and converged MEP.

moving, e.g., from t-site 1 to t-site 2 or 4. Starting from a linear interpolation guess for the MEP, stretching from initial to final t-sites, Fig. 5(b) shows the energy profile for the converged MEP. We find a diffusion barrier of 0.088 eV. Using harmonic transition-state theory⁴⁴ in the classical limit and the random-walk model of interstitial diffusion in a bcc lattice,⁴⁵ D_0 in the Arrhenius expression for the temperature-dependence of the diffusion constant $D = D_0 \exp(-E_a/k_B T)$ can be expressed as $D_0 = \frac{n}{6} a^2 \prod_{j=1}^{3N} \nu_j / \prod_{j=1}^{3N-1} \nu_j^\dagger$. Here, n is a geometrical factor for the number of equivalent jump paths (4 for H in the t-site), a is the jump length, and ν_j and ν_j^\dagger are the real normal mode frequencies at the initial state and the transition state, respectively. Our calculations predict

$$D = 1.5 \times 10^{-7} \exp(-0.088 \text{ eV}/k_B T) \text{ m}^2 \text{ s}^{-1}. \quad (2)$$

The diffusion coefficients of H in Fe from numerous measurements show a large scatter, since H is easily trapped by impurities in Fe. Higher diffusion coefficients are obtained for purer and better recrystallized Fe samples. The resulting experimental diffusion barrier depends significantly on the purity of Fe used for the study. Typical E_a values range from 0.035 eV to 0.142 eV and D_0 from $3.35 \times 10^{-8} \text{ m}^2 \text{ s}^{-1}$ to $2.2 \times 10^{-7} \text{ m}^2 \text{ s}^{-1}$ for H diffusion in bcc Fe, as compiled by Hayashi and Shu⁴⁶ from ten research groups around the world, for temperatures as low as 233 K. Our predictions of E_a and D_0 fall into the experimental range.

Around room temperature, quantum corrections to the diffusion barrier should be necessary to account for the discreteness of H vibrational modes in the metal lattice. This can be accomplished by using quantum partition functions in classical transition-state theory, as shown by Le Claire,⁴⁷ Ebisuzaki, Kass, and O'Keefe,⁴⁸ and Katz, Gvinan, and Borg.⁴⁹ The modified classical theory of overbarrier jumps by Katz, Gvinan, and Borg has been shown to give a plausible description of H diffusion in bcc metals above 250 K (Ref. 50), so we use their approach here. One assumption they make is that the lattice vibrations are decoupled from the localized H vibrational modes. We think this assumption is reasonable for H diffusion in bcc Fe due to the much larger mass of Fe than that of H. The way we obtain H vibrational frequencies is actually based on this assumption, i.e., we only allow H to move when the finite-difference frequencies are calculated. Kehr⁵⁰ simplified the equation from Katz, Gvinan, and Borg based on another assumption that the lattice vibrations are the same in the minimum energy and saddle-point configurations. For bcc metals at room temperature, the limit of $h\nu_H \gg k_B T$ usually applies, where ν_H is the frequency of the localized H vibrational modes. We find for bcc Fe that $h\nu_H$ ranges from 0.12 eV to 0.24 eV, which is indeed much greater than $k_B T$ at room temperature (~ 0.025 eV). According to Kehr,⁵⁰ in the limit of $h\nu_H \gg k_B T$, the diffusion coefficient can be expressed as

$$D = \frac{n}{6} a^2 \frac{k_B T}{h} \exp[-(\Delta E + \Delta \text{ZPE})/k_B T]. \quad (3)$$

Here ΔE is the energy difference between the saddle point and minimum energy configuration on the potential energy

surface (0.088 eV in our case), while ΔZPE is the difference in zero-point energies. The exponential term $(\Delta E + \Delta \text{ZPE})$ in Eq. (3) can be interpreted as a ZPE-corrected diffusion barrier. Since the minimum energy configuration contains one more degree of freedom, ΔZPE is usually negative (-0.046 eV in our case), leading to a decreased barrier. We obtain a ZPE-corrected diffusion barrier of 0.042 eV, indicating that the diffusion barrier is lowered by ZPE as temperature decreases. Moreover, the preexponential factor in Eq. (3) becomes temperature dependent, but is independent of isotope mass or host lattice properties. This has been shown to be in fair agreement with experiment above 250 K (Ref. 50). To compare our ZPE-corrected diffusion equation with a specific measurement, we use Grabke and Riecke's work that yielded a barrier (0.043 eV) closest to our ZPE-corrected barrier, so that we may focus on comparing D_0 from experiment and theory.²³ They employed an electrochemical permeation method to study H diffusion in very pure Fe in the temperature range of 283–348 and obtained a D_0 of $5.12 \times 10^{-8} \text{ m}^2 \text{ s}^{-1}$. Using an average temperature of 315 K, we obtain from Eq. (3) a pre-exponential factor of $4.4 \times 10^{-8} \text{ m}^2 \text{ s}^{-1}$, in good agreement with experiment.

Figure 5(b) also shows the local structures along the MEP for H moving from t-site 1 to t-site 2. The local structure of the transition state shows that H is at the center of the triangle comprised of Fe3, Fe5, and Fe6 [Fig. 5(c)]. To see whether H moves linearly from t-site 1 to t-site 2, we plot the coordinates (x and y) for all the images in Fig. 5(d). One can see that the path is not linear, but curved toward the o-site in the center [the path is schematically shown in a curved line in Fig. 5(a)].

We also explored another diffusion path in which H moves from t-site 1 to t-site 3 via the o-site in the middle [Fig. 5(a)]. We find that the path is linear, the o-site is a saddle point, and the diffusion barrier is 0.12 eV, which is just the energy difference between o-site and t-site shown in Table II. Analysis of the Hessian (energy second derivative) matrix shows that the o-site is actually a rank-2 saddle point, so it is not a true transition state. Walch also found that the o-site is actually a local maximum for H in his Hartree-Fock cluster study.⁸ We note that the t-o-t diffusion path has been proposed to contribute to the increase of the diffusion barrier at higher temperatures by some experimentalists.⁵¹

Quantum diffusion can be the dominant mechanism for H diffusion in metals at low temperatures.^{52,53} Several quantum theories of light atom interstitial diffusion in metals have been developed, such as the small polaron theory^{54,55} and phonon-assisted tunneling theory⁵⁶ to understand H diffusion in metals at low temperatures. However, the crossover between the classical and quantum regimes of hydrogen diffusion in bulk metals is not as straightforwardly obtained as that for H diffusion on metal surface.^{57–59} Quantum-diffusion theories have been applied mainly to H diffusion in metals, such as V, Nb, and Ta, where low-temperature (< 10 K) data are available.⁵² However, such data are lacking for Fe, partly due to the extremely low H solubility in bcc Fe at low temperatures.

Our results indicate that H has a high mobility in bulk bcc Fe while it prefers to stay on the surface instead of the bulk. Therefore, defect-free Fe will not effectively retain H in the

bulk to affect its mechanical properties. Trapping sites become important here. One type of trapping site is a vacancy, which can retain H atoms. Recently, Tateyama and Ohno⁶⁰ studied H-vacancy complexes in bcc Fe with periodic DFT-GGA. In agreement with our work, they found that H resides in the t-site of bcc Fe with a ~ 0.30 eV heat of solution. Moreover, they found that the monovacancy-H₂ (VH₂) configuration is the most favorable among all the VH_x (x from 1 to 6) complexes, instead of VH₆ as conventionally accepted. Interestingly, this VH₂ configuration can be related to our investigation of H on Fe(100). Suppose the monovacancy is at the body center of the bcc cubic unit cell (see Fig. 1). H atoms will reside in between the body center and the face center for VH_x. If we think of this monovacancy as an inner surface, H atoms actually reside at hollow sites of the inner surface, which resembles Fe(100). The VH₂ state has a formation energy of ~ 0.30 eV/H exothermic, which is actually very close to the adsorption of the H atom in the hollow site of Fe(100) (Table I). So our work provides a sound basis for the results found by Tateyama and Ohno regarding H-vacancy complexes in bcc Fe.

IV. SUMMARY AND CONCLUSIONS

We performed all-electron periodic DFT-GGA calculations of the adsorption of H on Fe(100), the absorption of H into Fe(100) and Fe(110) subsurfaces, and the dissolution energetics of H in ferromagnetic (FM) bcc Fe. We also studied the diffusion of H into bulk Fe from Fe(110) and Fe(100) and the diffusion of H in bulk Fe. We find that H prefers the threefold site on Fe(110) and the fourfold hollow site on Fe(100). For H in bulk Fe, we show that H prefers to stay in the t-site; the o-site may be destabilized because of the large expansion of the lattice required in order to accommodate the H atom. The dissolution energy of H in the t-site changes only slightly with H concentration, indicating a lack of significant H-H interactions in bulk Fe. The dissolution energy of H in the t-site is calculated to be 0.30 eV/atom endothermic, which agrees very well with experiment and an earlier DFT-GGA prediction. Slight charge transfer of ~ 0.10 e from Fe to H is found for both the o-site and the t-site. For H in Fe(110) and Fe(100) subsurfaces, we find that H stays at a t-site ~ 1.46 Å below the surface Fe(110) layer, but only ~ 0.35 Å below the surface Fe(100) layer. Diffusion to subsurface layers is endothermic in both cases, with barriers of 1.02 eV for Fe(110) and 0.38 eV for Fe(100). Thus, it is much easier for H to diffuse into bulk Fe from the (100) surface than from the (110) surface. The reverse process of H diffusion from Fe(110) and Fe(100) subsurfaces back to the surface has only a very small barrier ~ 0.03 eV. For a very dilute concentration of H (a Fe₁₂₈ supercell), the minimum energy path (MEP) of bulk H diffusion shows a barrier of

0.088 eV, in agreement with experimental values that show a rather large uncertainty (0.035–0.14 eV), caused by the large scatter in the measured diffusion coefficients. Taking into account the quantum discreteness of localized H vibrations, we obtain a zero-point-energy-corrected barrier of 0.042 eV with a preexponential factor of $\sim 4 \times 10^{-8}$ m² s⁻¹, in good agreement with room temperature measurements. We find that H does not utilize a straight-line trajectory, but rather hops from one t-site to a nearby t-site by a curved path distorted toward the o-site. We also find that diffusion via the o-site has a higher barrier and involves a rank-2 saddle point, suggesting that diffusion will not occur through the o-site.

Our study offers the following general conclusions: (i) H prefers to stay on Fe surfaces instead of bulk; (ii) Fe is a poor endothermic absorber of hydrogen because of the smallness of the interstices in Fe; (iii) the diffusion of H into Fe subsurfaces is much more difficult than the reverse process; (iv) the diffusion of H into Fe subsurfaces has a much lower barrier on Fe(100) than Fe(110); (v) the mobility of H in pure bcc Fe is very high due to the low diffusion barrier; (vi) the all-electron DFT-GGA approach yields adsorption, dissolution, and diffusion energetics that agree quite well with experiment, while providing a clear picture of the diffusion pathway and the reasons behind hydrogen's low solubility in Fe.

Because of the importance of understanding H embrittlement of steel, H in Fe has been the subject of intense study. The uniqueness of the H/Fe system lies in the very small lattice parameter of bcc Fe, namely, the small interstitial space yet close nearest-neighbor interstitial distance, which leads to low H solubility but high mobility. As a result, H will quickly migrate to surfaces or reach trapping sites, which could be crack tips, vacancies, grain boundaries, or alloying elements. In this case, even small concentrations of H can act as a strong embrittler because the local concentrations at crystalline defects could be high. These ideas of how H is able to embrittle Fe may be relevant to hydrogen embrittlement of transition metals from groups 6 and 8–11 (except Pd) in the periodic table. These transition metals have relatively small lattice parameters compared with other transition metals of the same structure, and they all show a positive enthalpy of solution.⁵² However, our general conclusions regarding H/Fe energetics may not be relevant for transition metals in groups 3–5 or lanthanides, which tend to have large lattice parameters, high H solubility, and form hydrides at ambient conditions.

ACKNOWLEDGMENTS

We thank the Army Research Office for funding and the Maui High Performance Computing Center and the NAVO MSRC for CPU time.

- ¹H. G. Nelson, in *Treatise on Materials Science and Technology*, edited by C. L. Briant and S. K. Banerji (Academic Press, New York, 1983), Vol. 25, p. 275.
- ²N. Eliaz, A. Shachar, B. Tal, and D. Eliezer, *Eng. Fail. Anal.* **9**, 167 (2002).
- ³R. A. Oriani, J. P. Hirth, and M. Smialowski, *Hydrogen Degradation of Ferrous Alloys* (Noyes Publications, Park Ridge, NJ, 1985).
- ⁴J. C. J. McMahon, in *Innovations in Ultrahigh-Strength Steels, Proceedings of the 34th Sagamore Army Materials Research Conference*, edited by G. B. Olson, M. Azrin, and E. S. Wright (Government Printing Office, Washington, DC, 1990), p. 597.
- ⁵D. E. Jiang and E. A. Carter, *Surf. Sci.* **547**, 85 (2003).
- ⁶W. Nichtl-Pecher, J. Gossman, L. Hammer, K. Heinz, and K. Müller, *J. Vac. Sci. Technol. A* **10**, 501 (1992).
- ⁷P. B. Merrill and R. J. Madix, *Surf. Sci.* **347**, 249 (1996).
- ⁸S. P. Walch, *Surf. Sci.* **143**, 188 (1984).
- ⁹M. Eder, K. Terakura, and J. Hafner, *Phys. Rev. B* **64**, 115426 (2002).
- ¹⁰J. P. Hirth, *Metall. Trans. A* **11A**, 861 (1980).
- ¹¹R. Griessen, *Phys. Rev. B* **38**, 3690 (1988).
- ¹²A. D. Vita and M. J. Gillan, *J. Phys.: Condens. Matter* **4**, 599 (1992).
- ¹³S. Philipp, R. L. Leibrich, P. C. Schmidt, and A. Weiss, *Ber. Bunsenges. Phys. Chem.* **96**, 1639 (1992).
- ¹⁴J. K. Nørskov, *Phys. Rev. B* **26**, 2875 (1982).
- ¹⁵M. J. Puska and R. M. Nieminen, *Phys. Rev. B* **29**, 5382 (1984).
- ¹⁶A. L. Companion and F. Liu, *J. Less-Common Met.* **107**, 131 (1985).
- ¹⁷C. Minot and C. Demangeat, *J. Chem. Phys.* **86**, 2161 (1987).
- ¹⁸A. Juan and R. Hoffmann, *Surf. Sci.* **421**, 1 (1999).
- ¹⁹X. Gong, Z. Zeng, and Q. Zheng, *J. Phys.: Condens. Matter* **1**, 7577 (1989).
- ²⁰K. Miwa and A. Fukumoto, *Phys. Rev. B* **65**, 155114 (2002).
- ²¹D. Vanderbilt, *Phys. Rev. B* **41**, 7892 (1990).
- ²²A. San-Martin and F. D. Manchester, in *Phase Diagrams of Binary Iron Alloys*, edited by H. Okamoto (ASM International, Materials Park, OH, 1993), p. 161.
- ²³H. J. Grabke and E. Riecke, *Mater. Technol.* **34**, 331 (2000), and references within.
- ²⁴J. Völkl and G. Alefeld, in *Hydrogen in Metals I*, edited by G. Alefeld and J. Völkl (Springer, Berlin, 1978), p. 321.
- ²⁵W. Windl, M. M. Bunea, R. Stumpf, S. T. Dunham, and M. P. Masquelier, *Phys. Rev. Lett.* **83**, 4345 (1999).
- ²⁶N. Sandberg, B. Magyari-Köpe, and T. R. Mattsson, *Phys. Rev. Lett.* **89**, 065901 (2002).
- ²⁷R. J. Needs, *J. Phys.: Condens. Matter* **11**, 10437 (1999).
- ²⁸D. E. Jiang and E. A. Carter, *Phys. Rev. B* **67**, 214103 (2003).
- ²⁹P. Hohenberg and W. Kohn, *Phys. Rev.* **136B**, 864 (1964).
- ³⁰W. Kohn and L. J. Sham, *Phys. Rev.* **140A**, 1133 (1965).
- ³¹J. P. Perdew, K. Burke, and M. Ernzerhof, *Phys. Rev. Lett.* **77**, 3865 (1996).
- ³²G. Kresse and J. Hafner, *Phys. Rev. B* **48**, 13115 (1993).
- ³³G. Kresse and J. Furthmüller, *Phys. Rev. B* **54**, 11169 (1996).
- ³⁴G. Kresse and J. Furthmüller, *Comput. Mater. Sci.* **6**, 15 (1996).
- ³⁵P. E. Blöchl, *Phys. Rev. B* **50**, 17953 (1994).
- ³⁶G. Kresse and D. Joubert, *Phys. Rev. B* **59**, 1758 (1999).
- ³⁷C. Kittel, *Introduction to Solid State Physics*, 7th ed. (Wiley, New York, 1996).
- ³⁸H. C. Herper, E. Hoffmann, and P. Entel, *Phys. Rev. B* **60**, 3839 (1999).
- ³⁹M. Methfessel and A. T. Paxton, *Phys. Rev. B* **40**, 3616 (1989).
- ⁴⁰G. Kresse and J. Hafner, *Surf. Sci.* **459**, 287 (2000).
- ⁴¹K. P. Huber and G. Hertzberg, *Molecular Spectra and Molecular Structure IV: Constants of Diatomic Molecules* (Van Nostrand Reinhold, New York, 1979).
- ⁴²G. Henkelman, B. P. Uberuaga, and H. Jónsson, *J. Chem. Phys.* **113**, 9901 (2000).
- ⁴³H. Jónsson, G. Mills, and K. W. Jacobsen, in *Classical and Quantum Dynamics in Condensed Phase Simulations*, edited by B. J. Berne, G. Ciccotti, and D. F. Coker (World Scientific, Singapore, 1998), p. 385.
- ⁴⁴G. H. Vineyard, *J. Phys. Chem. Solids* **3**, 121 (1957).
- ⁴⁵C. Wert and C. Zener, *Phys. Rev.* **76**, 1169 (1949).
- ⁴⁶Y. Hayashi and W. M. Shu, *Solid State Phenom.* **73–75**, 65 (2000).
- ⁴⁷A. D. Le Claire, *Philos. Mag.* **14**, 1271 (1966).
- ⁴⁸Y. Ebisuzaki, W. J. Kass, and J. O'Keeffe, *J. Chem. Phys.* **46**, 1373 (1967).
- ⁴⁹L. Katz, M. Guinan, and R. J. Borg, *Phys. Rev. B* **4**, 330 (1971).
- ⁵⁰K. W. Kehr, in *Hydrogen in Metals I*, edited by G. Alefeld and J. Völkl (Springer, Berlin, 1978), p. 197.
- ⁵¹R. B. Mclellan, *Scr. Metall.* **18**, 1017 (1984).
- ⁵²Y. Fukai, *The Metal-Hydrogen System* (Springer, Berlin, 1993).
- ⁵³H. Grabert and H. R. Schober, in *Hydrogen in Metals III*, edited by H. Wipf (Springer, Berlin, 1997), p. 5.
- ⁵⁴J. Yamashita and T. Kurosawa, *J. Phys. Chem. Solids* **5**, 34 (1958).
- ⁵⁵T. Holstein, *Ann. Phys. (San Diego)* **8**, 325 (1959).
- ⁵⁶C. P. Flynn and A. M. Stoneham, *Phys. Rev. B* **1**, 3966 (1970).
- ⁵⁷R. DiFoggio and R. Gomer, *Phys. Rev. B* **25**, 3490 (1982).
- ⁵⁸G. X. Cao, E. Nabighian, and X. D. Zhu, *Phys. Rev. Lett.* **79**, 3696 (1997).
- ⁵⁹L. J. Lauhon and W. Ho, *Phys. Rev. Lett.* **85**, 4566 (2000).
- ⁶⁰Y. Tateyama and T. Ohno, *Phys. Rev. B* **67**, 174105 (2003).